

Physical properties and magnetic structure of TbRhIn₅ intermetallic compound.

R. Lora-Serrano,¹ C. Giles,¹ E. Granado,^{1,2} D. J. Garcia,¹ E. Miranda,¹
O. Agüero,¹ L. Mendonça Ferreira,¹ J. G. S. Duque,¹ and P. G. Pagliuso¹

¹*Instituto de Física "Gleb Wataghin", UNICAMP, 13083-970, Campinas-SP, Brazil.**

²*Laboratório Nacional de Luz Síncrotron, Caixa Postal 6192, CEP 13084-971 Campinas-SP, Brazil*
(Dated: September 10, 2018)

In this work we report the physical properties of the new intermetallic compound TbRhIn₅ investigated by means of temperature dependent magnetic susceptibility, electrical resistivity, heat-capacity and resonant x-ray magnetic diffraction experiments. TbRhIn₅ is an intermetallic compound that orders antiferromagnetically at $T_N = 45.5$ K, the highest ordering temperature among the existing RRhIn₅ (1-1-5, R = rare earth) materials. This result is in contrast to what is expected from a de Gennes scaling along the RRhIn₅ series. The X-ray resonant diffraction data below T_N reveal a commensurate antiferromagnetic (AFM) structure with a propagation vector $(\frac{1}{2} 0 \frac{1}{2})$ and the Tb moments oriented along the c -axis. Strong (over two order of magnitude) dipolar enhancements of the magnetic Bragg peaks were observed at both Tb absorption edges L_{II} and L_{III} , indicating a fairly high polarization of the Tb 5d levels. Using a mean field model including an isotropic first-neighbors exchange interaction (J_{R-R}) and the tetragonal crystalline electrical field (CEF), we were able to fit our experimental data and to explain the direction of the ordered Tb-moments and the enhanced T_N of this compound. The evolution of the magnetic properties along the RRhIn₅ series and its relation to CEF effects for a given rare-earth is discussed.

PACS numbers: 75.50.Ee, 75.30.Gw, 75.10.Dg, 75.20.En

I. INTRODUCTION

The discovery of new series of structurally related compounds with novel physical behavior is an important approach to explore fundamental problems in the physics of highly correlated electron systems. Such problems include the interplay between superconductivity, magnetism and heavy fermion behavior in structurally related materials.^{1,2} Although the microscopic origin of this interplay remains a mystery, the search for new heavy fermion superconductors (HFS) is partially guided by the knowledge that certain structures favor the formation of this heavy electron ground state. Remarkable examples of related physical properties occurring in structurally related compounds are the series Ce_mMIn_{3m+2} ($M = Co, Rh$ or $Ir, m = 1, 2$)^{3,4,5,6,7} and their Pu-based analogs $PuMGa_5$.^{8,9,10} These materials grow in a tetragonal variant of the Cu_3Au -type structure and can be viewed as layers of a cubic cell ($CeIn_3$ or $PuGa_3$) stacked sequentially along the c -axis with intervening layers of $M(In, Ga)_2$.¹¹ The discovery of unconventional superconductivity (USC) in many of these compounds is an exciting opportunity to further explore the possibility of magnetically mediated superconductivity in strongly correlated electrons systems and its relationship with dimensionality and crystal structures. For instance, systematic alloying studies in $CeRh_{1-x}Ir_xIn_5$ ^{12,13} and $PuCo_{1-x}Rh_xGa_5$ ⁹ ($PuCoGa_5$ possesses the highest superconducting transition temperature, $T_c = 18$ K, among the pure Pu-based compounds⁸) have revealed an intriguing linear dependence between T_c and the ratio of the tetragonal lattice parameters c/a at ambient pressure, indicating that the increasing of the quasi-2D character of their crystal structure may favor USC.

Such as the high- T_c and the organic superconductors, HFS are believed to be magnetically mediated superconductors.¹⁴ Furthermore, in most cases, USC seems to occur at the vicinity of a magnetically ordered state and the spin fluctuations (SF) associated with this magnetic phase may mediate the superconducting pair formation.¹⁴ More recently, a bridge connecting the HFS and high- T_c superconductors (HTSC) has been proposed by NMR studies in $PuCoGa_5$. These studies have shown that superconductivity in this material is unconventional with d-wave symmetry and similar properties to those found in other HFS and HTSC, suggesting that these classes of complex USC may share the same pairing mechanism.¹⁰

Focusing our attention now to the Ce-based HFS, the magnetic properties of these materials are associated with their 4f electrons. Although these compounds display obvious heavy-fermion behavior, evidences for low-temperature 4f local moment behavior has also been found in this family.^{15,16,17} This apparent contradiction is directly related to an open question in condensed matter physics regarding the details of the crossover between quasi-localized 4f electron magnetic behavior at high-T to a renormalized heavy-electron state at lower temperatures. However, if certain structures favor USC mediated by magnetic fluctuations, it is an important first step to understand how layered structures can affect CEF anisotropy, magnetic exchange and/or anisotropic transport properties (quasi-2D band-structure). In this regard, detailed studies of the 4f electrons magnetism along the series of rare-earth and actinides based 1-1-5 compounds may be very elucidative.

In the case of the Ce-based compounds, their Nd-, Sm- and Gd-based structurally related magnetic mate-

rials have been studied in detail.^{18,19,20,21,22,23,24} It has been found that the magnetic properties of these non-Ce analogs mainly depend on the interplay between CEF effects and exchange magnetic interaction. For example, among the Nd-based compounds NdMIn₅ and Nd₂MIn₈ analogs for M = Rh or Ir, it was found a systematic relationship between the AFM ordering temperature T_N and the low- T CEF splitting.¹⁹ Besides, when the magnetic properties of the tetragonal variants NdMIn₅ and Nd₂MIn₈ are compared to that for its cubic NdIn₃, T_N is enhanced by a factor of two.^{13,19,25} In contrast, the tetragonal CeRhIn₅ and Ce₂RhIn₈ present a T_N a factor of two smaller than that for CeIn₃ whereas for the Gd-based tetragonal materials the low temperature magnetic properties remain nearly unaltered compared to the GdIn₃.^{13,19,21} Finally, the resolved magnetic structures for some of these compounds have revealed that the rare-earth magnetic moments lie in the ab -plane for CeRhIn₅ and GdRhIn₅ compounds and point along the c -axis for NdRhIn₅ tetragonal materials.^{21,22,23,24}

To further explore the trends in the evolution of the magnetic properties within the series, particularly for the RRhIn₅ compounds, we have investigated the physical properties and magnetic structure of a new member of this series, TbRhIn₅. It was found to be an intermetallic compound that orders antiferromagnetically at $T_N \sim 46$ K, the highest ordering temperature among the existing RRhIn₅ materials. The magnetic structure of TbRhIn₅, resolved using Resonant X-ray Magnetic Diffraction (RXMD) experiments, is commensurate with propagation vector $\tau = (\frac{1}{2} \ 0 \ \frac{1}{2})$ and the Tb moments oriented along the c -axis. The direction of the ordering Tb moments and the enhanced T_N of this compound were successfully explained by a mean field model including an isotropic first-neighbors exchange interaction (J_{R-R}) and the tetragonal CEF, and was used to fit the magnetic susceptibility and specific heat experimental data.

Besides revealing the magnetic properties of this novel compound, the reported results confirm the CEF driven T_N behavior and the direction of ordered moments observed in other members of the series. We discuss also the particular case where the rare-earth moments order out of the c -axis, for which T_N can be reduced by tuning the CEF parameters. This fact represents an interesting frustration mechanism that may play some role in the origin of the relevant low-dimensional SF in complex classes of materials such as the Ce_{*m*}MIn_{3*m*+2} (M = Rh, Ir and Co; $m = 1, 2$) HFS.

II. EXPERIMENT

Single crystals of TbRhIn₅ with dimensions up to 2 cm³ approximately were grown from In-flux, as reported previously.^{3,4,5} Most of the crystals show columnar habit, with their long axis along the tetragonal c -axis. The tetragonal HoCoGa₅-type structure¹¹ with cell parameters $a = 4.595(4)$ Å and $c = 7.418(4)$ Å were confirmed by

x-ray powder diffraction and the crystal orientation was determined by the usual Laue method. Specific heat measurements were performed in a Quantum Design PPMS small-mass calorimeter that employs a quasi-adiabatic thermal relaxation technique. Magnetization measurements were made in a Quantum Design *dc* Superconducting Quantum Interference Device and electrical resistivity was measured using the PPMS low-frequency *ac* resistance bridge and four-contact configuration. The samples used in the electrical resistivity measurements were previously screened for In-free surface contamination.

RXMD measurements were carried out at the bending magnet beamline XRD2 of the Brazilian Synchrotron Light Source (LNLS), in Campinas, Brazil using a double-bounce Si (111) monochromator, with sagittal focusing.²⁶ A Rh-coated mirror was used to vertically focus the beam and also to eliminate third and higher-order harmonics in the incident beam. The bending magnet source delivers photon beams with a flux of $\sim 3 \times 10^{10}$ photons/s around 8 keV at 100 mA in spot of ~ 0.6 mm (vertical) x 2.0 mm (horizontal) at the sample, with an energy resolution from the source of $\frac{\delta E}{E} \sim 10^{-4}$. Our experiments were performed in the vertical scattering plane, i.e, perpendicular to the linear polarization of the incident photons (σ polarization²⁷).

Although neutron diffraction is the natural choice of experiments to resolve magnetic structures, RXMD offers the advantage that only very small samples are required. For the RXMD experiments the high resolution of the magnetic reflections is obtained as a natural consequence of the intrinsic collimation of the synchrotron x-ray source, and the small cross section ensures that even for strong magnetic Bragg peaks, the intensity is not extinction limited and a reliable measurement of the order parameter is possible. In our experiments high count rates were obtained, allowing a precise temperature dependence of the ordered Tb moments.

A platelet of TbRhIn₅, from the same batch as that used for macroscopic properties measurements, was mechanically polished perpendicular to c -axis ((0 0 1) flat surface) to eliminate surface contamination from the residual flux and to increase the reflectivity, which gives a mosaic spread characterized by the full width at half maximum (FWHM) of $\sim 0.04^\circ$. The sample was cut parallel to the ab -plane to have a final shape of a long block with dimensions of 4x3x1 mm³ and to investigate reflections in the $[h \ 0 \ l]$ zone axis. The size of the sample was chosen to ensure that the beam completely reaches the crystal in the scattering plane for all angles of interest. The sample was mounted on the cold finger of a closed-cycle He cryostat (base temperature 11 K) with a cylindrical Be window.

III. RESULTS

The temperature dependence of the magnetic susceptibility measured for a magnetic field $H = 1$ kOe applied parallel $\chi_{//}$ and perpendicular χ_{\perp} to the c -axis is presented in Fig. 1(a). Fig. 1(b) shows the polycrystalline average of Fig. 1(a) data taken as $\chi_{poly} = (\chi_{//} + 2\chi_{\perp})/3$.

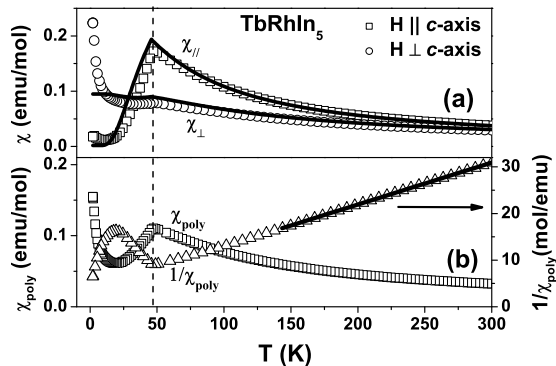


FIG. 1: (a) Temperature dependence of the magnetic susceptibility for TbRhIn₅, for $H = 1$ kOe applied parallel ($\chi_{//}$) (open squares) and perpendicular to the c -axis (χ_{\perp}) (open circles). The solid lines are best fits to the data for both directions using our mean field model (see below). (b) $\chi_{poly}(T)$ and the inverse $1/\chi_{poly}(T)$; The solid line is the linear fit to the $1/\chi_{poly}$ data for $T > 140$ K. From this fit we extracted $\mu_{eff} = 9.4(1)\mu_B$ and $\theta = -47(1)$ K for TbRhIn₅.

From a linear fit to the inverse of $\chi_{poly}(T)$ for $T > 140$ K using a Curie-Weiss law, we have obtained a Curie-Weiss temperature $\theta = -47(1)$ K and the Tb³⁺ effective magnetic moment $\mu_{eff} = 9.4(1)\mu_B$. As it can be seen in Fig. 1(a) the magnetic susceptibility of TbRhIn₅ is higher for the field applied along the c -axis, in agreement to what was found for all others non-S R-members of these series.^{3,18,19} The ratio $\chi_{//}/\chi_{\perp} \sim 2.08$ taken at T_N is mainly determined by the tetragonal CEF and it reflects the same order of magnetic anisotropy found for other members of these series.^{3,18,19} The solid lines in Fig. 1(a) are the best fits to the data using a mean field model which includes an isotropic first-neighbors exchange interaction and the tetragonal CEF.²⁸ The best fit yields a $J_{R-R} = 0.2$ meV (J_{R-R} is equal to zK_{RKKY} in the notation of Ref. 28) for the exchange parameter and the CEF parameters $B_{20} = -1.4 \times 10^{-1}$ meV, $B_{40} = 1.3 \times 10^{-4}$ meV, $B_{44} = -5.3 \times 10^{-3}$ meV, $B_{60} = 0.21 \times 10^{-4}$ meV, $B_{64} = 1.5 \times 10^{-4}$ meV. The CEF level scheme obtained from the splitting of the Tb³⁺ ($J = 6$) multiplet by above parameters is built up of three doublets and seven singlets with an overall splitting of roughly 310 K. The calculated curves using our model reproduce very well the magnetic anisotropy and the peak of the magnetic susceptibility at $T_N \sim 45.5$ K for both directions (Fig. 1(a)). At lower- T an intrinsic and anisotropic

Curie-like tail can be seen in the magnetic susceptibility data and it is presumably associated with an additional magnetic transition with changes in the magnetic structure which happens within the ordered state (similarly to TbIn₃ cubic compound at higher temperatures^{25,29}).

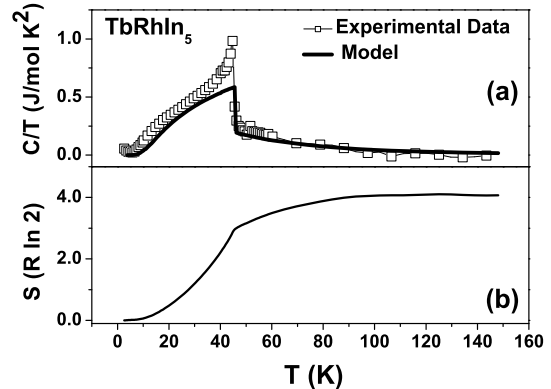


FIG. 2: (a) Specific-heat data divided by temperature as a function of temperature for a single crystal of TbRhIn₅. The solid line is the best fit to this data using our mean field model. (b) The corresponding magnetic entropy in the temperature range $2 < T < 150$ K for TbRhIn₅.

Fig. 2(a) shows the specific heat divided by temperature and the corresponding magnetic entropy (Fig. 2(b)) in the temperature range $0 < T < 150$ K for TbRhIn₅. To calculate the magnetic entropy, the phonon contribution was estimated from the non-magnetic specific-heat data of YRhIn₅ and subtracted from the total specific heat of the magnetic compound. The recovery magnetic entropy at high- T is close to its expected values for $J = 6$. An anomaly in the specific-heat data associated with the onset of AFM order can be seen at $T_N = 45.5$ K in good agreement with the temperatures where the maximum in the magnetic susceptibility occurs (see Fig. 1). Again, the solid line in Fig. 2(a) represents the best fit to the data using our mean field model for the same parameters used in the fit of the $\chi(T)$ data (the best set of parameters was obtained from simultaneous minimization process for both $\chi(T)$ and $C/T(T)$ data).

The temperature dependence of the electrical resistivity for TbRhIn₅ single crystals is plotted in Fig. 3. Among various measured crystals, the room temperature value of the resistivity ranges between $10 - 35 \mu\Omega$ cm indicating the high quality of the crystals. At high temperature the data always showed a metallic behavior while, at low temperatures, a clear kink can be seen at the ordering temperature T_N .

The c/a ratio and T_N values for RRhIn₅ compounds are shown in Fig. 4. The solid line in Fig. 4(a) is the expected behavior for T_N and θ according to de Gennes factor $(g_J - 1)^2 J(J+1)$ for the ground-state multiplet J of each rare earth normalized by their values for GdRhIn₅.

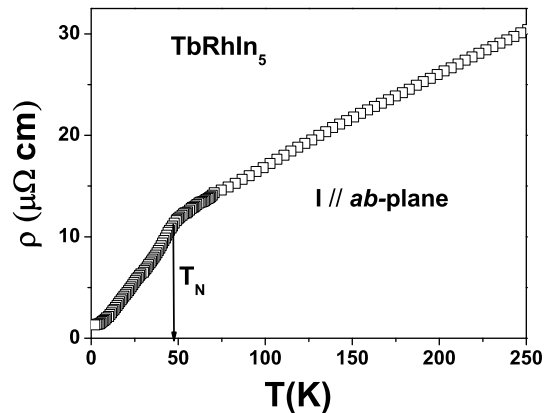


FIG. 3: Temperature dependence of the electrical resistivity for TbRhIn₅ single crystal. The current (\mathbf{I}) has been applied parallel to the ab -plane. The solid arrow point out a kink at the Néel temperature for this compound.

As for $R = \text{Ce}$ and Nd ,¹⁹ T_N of the TbRhIn₅ does not follow the de Gennes scaling. Interestingly, T_N for TbRhIn₅ is the highest among the existing RRhIn₅ members.

The microscopic low-temperature magnetism of TbRhIn₅ was further investigated by RXMD. For the sample orientation used in the experiments, with the zone axis $[h\ 0\ l]$ parallel to the scattering plane, the resonant scattering cross section (the non-resonant scattering contribution was observed to be negligible) for the case of a dipolar resonance with a linear polarized incident beam perpendicular to the scattering plane may be written as:^{27,30}

$$I \propto \left| \sum_n \hat{u}_n \cdot \hat{k}_f e^{i\mathbf{Q} \cdot \mathbf{r}_n} \right|^2 \quad (1)$$

where $\mathbf{Q} = \mathbf{k}_f - \mathbf{k}_i$ is the scattering vector, \hat{k}_f is the direction of the scattered wave vector \mathbf{k}_f , and \hat{u}_n is the moment direction at the n th site. The proportionality symbol \propto includes \mathbf{Q} -independent resonant amplitudes, the Lorentz factor, arbitrary scale factors and an angular correction factor for asymmetric reflections. The summation is over all the n th resonant ions in the magnetic unit cell and \mathbf{r}_n is the position of such an ion. Note that in the present geometry and in the absence of an in-plane π polarized component of the incident beam, the dipolar resonant cross section terms are not sensitive to the component of the ordered moment perpendicular to the scattering plane (i.e., along the b axis).

Below $T_N \sim 46$ K, careful scans along $[h\ 0\ l]$ direction revealed superstructure Bragg peaks of type $(\frac{2n+1}{2}\ 0\ \frac{2m+1}{2})$ (n, m integers), appearing as a result of the strong resonant enhancements of the magnetic peaks for both Tb L_{II} and L_{III} edges, and the high magnetic moment per Tb³⁺ ion of $\mu = 9.5 \mu_B$. In the low temperature phase, magnetic peaks $(0\ \frac{2n+1}{2}\ \frac{2m+1}{2})$ were also ob-

served, revealing a twinned magnetic structure. The intensities of $(\frac{2n+1}{2}\ 0\ \frac{2m+1}{2})$ and $(0\ \frac{2n+1}{2}\ \frac{2m+1}{2})$ were comparable, suggesting approximately equal domain population. Therefore, our magnetic cell is duplicated in the a and c directions when compared to the chemical one. Above T_N only charge peaks consistent with the tetragonal HoCoGa₅-type structure were observed. The widths (FWHM) of magnetic peaks were the same as that for equivalent scans through a charge Bragg peak.

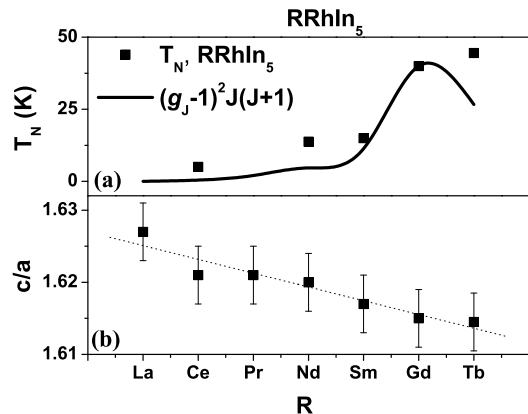


FIG. 4: T_N (a) and c/a ratio (b) for the RRhIn₅ compounds. The solid line in (a) represents the de Gennes factor $(g_J - 1)^2 J(J + 1)$ for the ground state multiplet J of the rare earth ions, normalized by the GdRhIn₅. The dashed line in (b) is just a guide to the eye.

The magnetic structure of TbRhIn₅ was then resolved from the obtained modulation vector $\tau = (\frac{1}{2}\ 0\ \frac{1}{2})$ and the magnetic moments direction was established by comparing the observed intensities of some magnetic Bragg reflections with a model based on the resonant cross section of Eq. 1. In Fig. 5, the integrated intensities of five magnetic reflections obtained at $T = 20$ K are shown with solid squares. We used asymmetric reflections (\mathbf{Q} vector out of scattering plane) of the type $(0\ \frac{2n+1}{2}\ \frac{2m+1}{2})$ in order to also analyze the b -axis component in the resonant cross section, which can not be distinguished with \mathbf{Q} vectors into the scattering plane (i.e. with $(\frac{2n+1}{2}\ 0\ \frac{2m+1}{2})$ reflections). Experimental reflections were taken at the maximum enhancement of magnetic signal at the L_{II} edge, $E = 8253$ eV, and the data has been numerically integrated using gaussian fit functions (solid squares in Fig. 5). Three possibilities were tested, a first one assuming the moments along the c -direction (solid line), a second with the moments aligned along the a -direction (dashed line) and a third one with the moments along b -direction (dashed-dotted line). As can be seen in Fig. 5 the model with the ordered moments $\hat{u}_i // c$ -direction is the one in agreement with the observed data. A similar trend was also observed for NdRhIn₅ family compound²⁴ in its low-temperature AFM phase with the moment locked in the c -axis. Given the experimental errors, the directions

of the ordered moments is determined within $\sim 10^\circ$ of the c -direction.

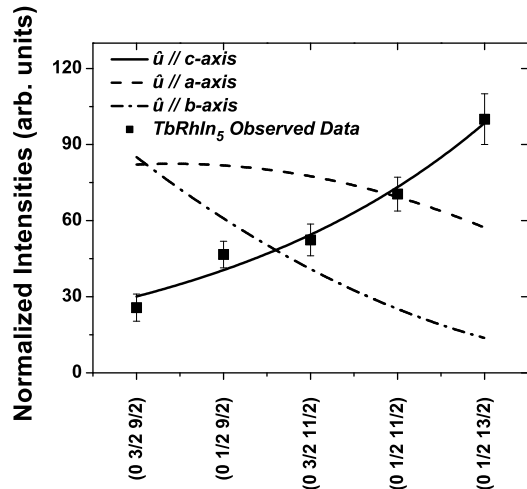


FIG. 5: Integrated intensities of five experimentally-obtained magnetic reflections for TbRhIn₅ (■) along with calculated intensities for a magnetic moment parallel to c -axis (solid line), to a (dashed line) and b -axis (dashed-dotted line).

In Fig. 6 the magnetic unit cell of TbRhIn₅ is shown according to results depicted in Fig. 5. A half magnetic cell is shown with moment directions at the Tb³⁺ ion crystallographic sites.

In order to use the resonant enhancement of the magnetic peaks, the primary beam energy was tuned to the L_{II} and L_{III} absorption edges of Tb³⁺ ion (tabulated as being 8252 eV and 7514 eV, respectively). In Figs. 7(a) and (b) we plot the scattered intensity of the $(\frac{1}{2} 0 \frac{11}{2})$ magnetic Bragg peak as a function of the incident photon energy on tuning through the L_{II} and L_{III} edges, respectively. The data were corrected for absorption (coefficient $\mu(E)$ is showed with the solid line curve and the right side scale in Figs. 7) using the fluorescence emission.³¹ The inflection points of $\mu(E)$ curves (vertical dashed line) were used to define the absorption edges. In both cases, the maximum resonant enhancement is observed ~ 2 eV above the edges, which is a signature of the electric dipole ($E1$) resonance involving electronic transitions $2p_{1/2} \leftrightarrow 5d$ and $2p_{3/2} \leftrightarrow 5d$. A remarkable enhancement of over two orders of magnitude for both edges has been obtained. From the fit to a Lorentzian-squared line profile, the width of resonance were found at both edges as being 6.2 eV and 6.4 eV for L_{II} and L_{III} , respectively (corrected for energy resolution).

The relative strength $I(L_{III})/I(L_{II})$ of the resonant enhancements (the “branching ratio”) of the $E1$ resonances is ~ 2.9 which is in agreement with the theoretical expectations for branching ratios at the rare-earth L edges. This ratio is of interest since it relates to the underlying electronic and magnetic structures (see Refs.

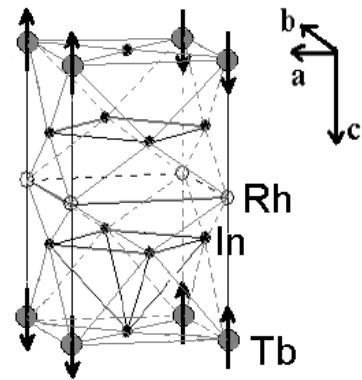


FIG. 6: The magnetic structure of TbRhIn₅ at 20 K. A half magnetic unit cell is shown. $\uparrow(\downarrow)$ represents the directions “up” (“down”) of magnetic moments of Tb (depicted by gray filled circles) along the c axis.

32 and 33 and the references cited therein for more details). According to Ref. 32, in heavy rare earth such as Tb, the $E1$ resonance at the L_{III} is ~ 2.5 times that of the L_{II} edge. This expectation is in agreement with our observations. Intensity oscillations have been observed above the edges, and can be ascribed to magnetic DAFS oscillations³⁴ (Diffraction Anomalous Fine Structure) which are oscillations of the anomalous scattering factors associated with the interference of the photoelectrons wave function with the surrounding atoms that bring a fine structure of oscillations in the energy line-shape spectrum.

The behavior of the ordered phase was measured as the temperature was raised at the L_{II} edge. The measurements of the integrated intensities were performed on the $(\frac{1}{2} 0 \frac{11}{2})$ satellite reflection. In Fig. 8 the data of longitudinal scans along this reflection is displayed as function of the reduced temperature T/T_N . As the temperature increases, the peak intensity gradually decreases and disappears above T_N . This result, as well as the one obtained for the energy dependence described above, clearly confirm the magnetic nature of the observed peaks. Data were taken on two regimes: on warming (filled circles on Fig. 8) and cooling (open circles). A fitting to the usual power-law expression ($\sim (1 - T/T_N)^{2\beta}$) for a second order phase transition (denoted by a solid line in the inset) within the temperature range of approximately 3% below T_N on the warming regime data gives a magnetic transition temperature $T_N = 45.56(2)$ K and a critical order exponent $\beta = 0.35(2)$ for the Tb sublattice magnetization. This value of β is compatible with a three-dimensional Heisenberg system. No hysteresis was observed around the ordering temperature and the smooth decreasing in intensity in the crossover to the paramagnetic phase is consistent with a second order transition.

In Table 1 we summarize the experimental parameters obtained for TbRhIn₅ in this work.

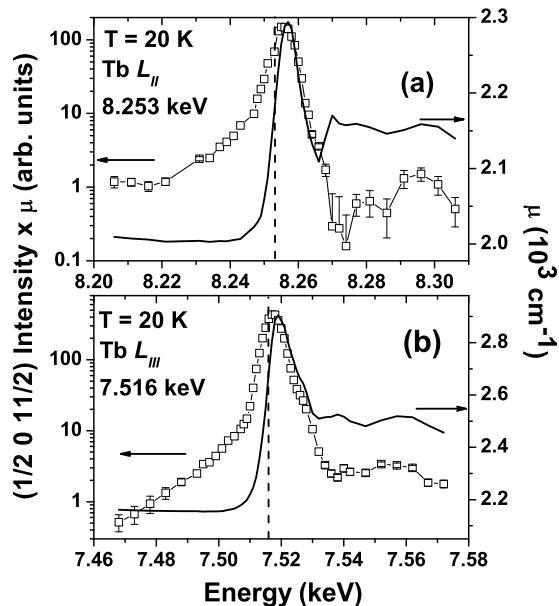


FIG. 7: Energy dependence of the $(\frac{1}{2} 0 \frac{1}{2})$ magnetic peak (open squares) through the Tb L_{II} (a) and L_{III} (b) edges. The open symbols are gaussian fit to the elastic peak at each energy used in the scan. The data have been corrected for absorption. Solid line curve represents $\mu(E)$ obtained from the fluorescent yield (scale on the right). From the $\mu(E)$ inflection points we determine the absorption edges values (vertical dashed line) as being 8253 eV (L_{II}) and 7516 eV (L_{III}).

IV. DISCUSSION

As discussed in the introduction, to follow the evolution of the $4f$ magnetism along the R_mMIn_{3m+2} series is a crucial first step to achieve a deeper understanding of the complex physical properties of these materials. Early comparative studies of the magnetic properties in this family have shown that for the Ce-based materials where the magnetic ordered moments are not aligned along the c -axis,²⁴ T_N is suppressed to less than 0.5 of the $CeIn_3$ value for $CeRhIn_5$ where the Ce magnetic moments lie in the ab -plane within the AFM state. On the other hand, for $NdRhIn_5$, where the ordered moments point along the c -axis materials,²⁴ T_N is significantly enhanced when compared to that for their cubic $NdIn_3$ parent compound. And lastly, for the Gd-based materials, where the CEF effects are small, the low temperature magnetic properties remain nearly unaltered compared to the $GdIn_3$,^{13,19,21} suggesting that the low temperature CEF scheme configuration plays a fundamental role in the observed trends.

Regarding the influence of a given CEF scheme in the AFM ordering temperature, it is reasonable to assume that if a system orders in a given direction and CEF parameters are modified making it more magnetically susceptible in some other direction, but without actually changing the order, the system may experiment some

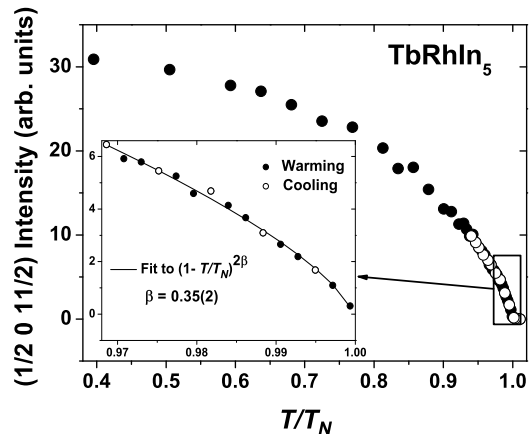


FIG. 8: Temperature dependence of the magnetic Bragg integrated intensities for $(\frac{1}{2} 0 \frac{1}{2})$ magnetic peak. The inset shows in details the critical region around the transition at the Néel temperature for this compound. From a power law fit to this data within the temperature range of approximately 3% below T_N we obtain a $T_N = 45.56(2)$ K and a critical parameter $\beta = 0.35(2)$

kind of magnetic frustration or the energy barrier between these states should diminish. Therefore, the ordering temperature should decrease as well. Inversely, if the system orders in a certain direction and CEF parameters change favoring even more this state, the ordering temperature should increase.

We have shown that this new member of the $RRhIn_5$, $TbRhIn_5$, orders antiferromagnetically at $T_N = 45.5$ K, which is an enhanced ordering temperature when compared to $T_N \sim 32$ K of $TbIn_3$. As $TbRhIn_5$ is more magnetically susceptible for a field applied along the c -axis, according to the scenario above, the Tb moment must be ordered along the c -axis to explain the enhanced T_N of $TbRhIn_5$.

Taking advantages of the higher Q resolution available with x-ray scattering techniques and using the RXMD cross section to determine moment directions in magnetic compounds,^{27,35} we resolved the magnetic structure of $TbRhIn_5$. Recently, this technique has been also successfully used to determine the magnetic structure of two Gd members of the R_mMIn_{3m+2} ($m = 1, 2$; $M = Rh, Ir$; $n = 1$) series.^{20,21}

As expected from the idea above, the solved magnetic structure of $TbRhIn_5$ reveals a commensurate AFM structure with propagation vector $(\frac{1}{2} 0 \frac{1}{2})$ and the Tb moments oriented along the c -axis (see Fig. 6). The direction of the ordered moments was established by comparing the observed intensities of five magnetic Bragg reflections (Fig. 5) with a model based on the resonant cross section for the case of dipolar resonance with a linear polarized incident beam perpendicular to the scattering plane (Eq. 1). The model considers the possible orienta-

TABLE I: Experimental parameters for TbRhIn₅.

$a(\text{\AA})$	$c(\text{\AA})$	$T_N(\text{K})$	$J_{R-R}(\text{meV})$	$\frac{T_{N,RRhIn_5}}{T_{N,RIn_3}}$	$B_{20}(\text{meV})$	$B_{40}(\text{meV})$	$B_{44}(\text{meV})$	$B_{60}(\text{meV})$	$B_{64}(\text{meV})$
4.595(3)	7.418(3)	45.5	0.2	1.39	-1.4×10^{-1}	1.3×10^{-4}	-5.3×10^{-3}	0.2×10^{-4}	1.5×10^{-4}

tion of the moments along the three tetragonal axis. In Fig. 5 it is obvious the agreement between experimental data and the model when the calculations were done assuming the moments along c -direction (solid line).

In addition, a proposed mean field model including an isotropic first-neighbors exchange interaction and the tetragonal CEF²⁸ has shown that the enhancement of T_N for tetragonal compounds that orders axially is a general trend for tetragonal materials when the CEF parameters tend to increase the fluctuations along the c -axis. We have used this model to fit our susceptibility and specific heat data, and we could successfully reproduce all the main features of our data, including the prediction of AFM ordering along the c -axis²⁸ for the CEF and J_{R-R} parameters given in Table 1.

Therefore, the reported magnetic properties of TbRhIn₅ compound is another experimental evidence of these general CEF induced trends along R_mMIn_{3m+2} ($m = 1, 2$; $M = \text{Rh, Ir}$). As such, with the CEF effects being very important in determining T_N , it is expected that the de Gennes scaling would fail to describe the behavior of T_N along the RRhIn₅ series (see Fig. 4).

It is important to note that this mean field model has also predicted that, for $J = 5/2$ and when the system spin is on the plane (for the Ce case) the Néel temperature approximately decreases when the CEF parameters increases fluctuations on c -axis, which is an effective measure of the system likeness to be in the c -direction. This prediction is consistent with the fact that the tetragonal CeRhIn₅ and Ce₂RhIn₈ present higher magnetic susceptibilities when magnetic field is applied along the c -axis and T_N a factor of two smaller than that for CeIn₃. It is obvious that the hybridization and Kondo effects are very important in the case of the Ce-based materials, but it is interesting to note that this CEF driven magnetic frustration mechanism combined to hybridization could create strong in-plane magnetic fluctuations that can mediate the quasi-2D unconventional superconductivity in these systems. It would be interesting to further test this model for others members of the R_mMIn_{3m+2} that present decreasing of T_N for tetragonal compounds. Although the effect is only about 20%, the tetragonal Sm-based compounds present smaller T_N values than their cubic rela-

tive SmIn₃.¹⁹ Therefore, according to the present model, the Sm-ordered moment for these materials should be aligned out of the c -axis, most likely in the ab -plane.

V. CONCLUSION

In conclusion, we have presented the physical properties and magnetic structure of a new member of the R_mMIn_{3m+2} series, TbRhIn₅. This intermetallic compound orders antiferromagnetically at $T_N = 45.5$ K, the highest ordering temperature among the existing RRhIn₅ materials. The solved magnetic structure of TbRhIn₅ is commensurate with propagation vector $\tau = (\frac{1}{2} \ 0 \ \frac{1}{2})$ and the Tb moments oriented along the c -axis. The direction of the ordering Tb-moments and the enhanced T_N of this compound were successfully explained by a mean field model including an isotropic first-neighbors exchange interaction and the tetragonal CEF. Also, the model reproduces all interesting features of our susceptibility and specific heat experimental data for the set of CEF parameters given in Table 1. We argue that reported magnetic properties of TbRhIn₅ compound is another experimental evidence of a more general CEF induced trend along the R_mMIn_{3m+2} ($m = 1, 2$; $M = \text{Rh, Ir}$). The particular case where the rare-earth moments ordered out of the c -axis and the T_N can be reduced by tuning the CEF parameters reveals a frustration mechanism that may play some role in producing in-plane magnetic fluctuations relevant to the physical properties of complex classes of materials such as the Ce_mMIn_{3m+2} ($M = \text{Rh, Ir and Co}$; $m=1,2$) HFS.

Acknowledgments

We thank A. O. G. Rodriguez and J. Madureira for helpful and interesting discussions about the magnetic moments orientation model. This work was supported by FAPESP (SP-Brazil) Grants No. 03/09861-7, 04/08798-2, 05/00962-0, 00/08649-6 and CNPq(Brazil) Grants No. 140613/2002-1, 307668/03, 04/08798-2 and 304466/20003-4. LNLS at Campinas is also acknowledged for beamtime at XRD2 beamline.

* Electronic address: rloraf@ifi.unicamp.br

¹ Z. Fisk, J. L. Sarrao, J. L. Smith, and J. D. Thompson, Proc. Natl. Acad. Sci. USA **92**, 6663 (1995).

² T. Moriya and K. Ueda, Rep. Prog. Phys. **66**, 1299 (2003).

³ H. Hegger, C. Petrovic, E. G. Moshopoulou, M. F. Hund-

ley, J. L. Sarrao, Z. Fisk, and J. D. Thompson, Phys. Rev. Lett. **84**, 4986 (2000).

⁴ C. Petrovic, R. Movshovich, M. Jaime, P. G. Pagliuso, M. F. Hundley, J. L. Sarrao, J. D. Thompson, and Z. Fisk, Europhys. Lett. **354-359**, 4986 (2001).

- ⁵ C. Petrovic, P. G. Pagliuso, M. F. Hundley, R. Movshovich, J. L. Sarrao, J. D. Thompson, Z. Fisk, and P. Monthoux, *J. Phys.: Condens. Matter* **13**, L337 (2001).
- ⁶ J. D. Thompson, R. Movshovich, Z. Fisk, F. Bouquet, N. J. Curro, R. A. Fisher, P. C. Hammel, H. Hegger, M. F. Hundley, M. Jaime, et al., *J. Magn. Magn. Mat.* **226-230**, 5 (2001).
- ⁷ G. Chen, S. Ohara, M. Hedo, Y. Uwatoko, K. Saito, M. Sorai, and I. Sakamoto, *J. Phys. Soc. Japan* **71**, 2836 (2002).
- ⁸ J. L. Sarrao, L. A. Morales, J. D. Thompson, B. L. Scott, G. R. Stewart, F. Wastin, J. Rebizant, P. Boulet, E. Colineau, and G. H. Lander, *Nature* **420**, 297 (2002).
- ⁹ E. D. Bauer, J. D. Thompson, J. L. Sarrao, L. A. Morales, F. Wastin, J. Rebizant, J. C. Griveau, P. Javorsky, P. Boulet, E. Colineau, et al., *Phys. Rev. Lett.* **93**, 147005 (2004).
- ¹⁰ N. J. Curro, T. Caldwell, E. D. Bauer, L. A. Morales, M. J. Graf, Y. Bang, A. V. Balatsky, J. D. Thompson, and J. L. Sarrao, *Nature* **434**, 622 (2005).
- ¹¹ E. G. Moshopoulou, Z. Fisk, J. L. Sarrao, and J. D. Thompson, *J. Solid State Chem.* **158**, 25 (2001).
- ¹² P. G. Pagliuso, C. Petrovic, R. Movshovich, D. Hall, M. F. Hundley, J. L. Sarrao, J. D. Thompson, and Z. Fisk, *Phys. Rev. B* **64**, 100503(R) (2001).
- ¹³ P. G. Pagliuso, R. Movshovich, A. D. Bianchi, M. Nicklas, J. D. Thompson, M. F. Hundley, J. L. Sarrao, and Z. Fisk, *Physica B* **312-313**, 129 (2002).
- ¹⁴ N. D. Mathur, F. M. Grosche, S. R. Julian, I. R. Walker, D. M. Freye, R. K. W. Haselwimmer, and G. G. Lonzarich, *Nature* **394**, 39 (1998).
- ¹⁵ T. Takeuchi, T. Inoue, K. Sugiyama, D. Aoki, Y. Tokiwa, Y. Haga, K. Kindo, and Y. Onuki, *J. Phys. Soc. Jpn* **70**, 877 (2001).
- ¹⁶ U. Alver, R. G. Goodrich, N. Harrison, D. W. Hall, E. C. Palm, T. P. Murphy, S. W. Tozer, P. G. Pagliuso, N. O. Moreno, J. L. Sarrao, et al., *Phys. Rev. B* **64**, 180402(R) (2001).
- ¹⁷ V. F. Correa, L. Tung, S. M. Hollen, P. G. Pagliuso, N. O. Moreno, J. C. Lashley, J. L. Sarrao, and A. H. Lacerda, *Phys. Rev. B* **69**, 174424 (2004).
- ¹⁸ P. G. Pagliuso, J. D. Thompson, M. F. Hundley, J. L. Sarrao, and Z. Fisk, *Phys. Rev. B* **63**, 054426 (2001).
- ¹⁹ P. G. Pagliuso, J. D. Thompson, M. F. Hundley, and J. L. Sarrao, *Phys. Rev. B* **62**, 12266 (2000).
- ²⁰ E. Granado, P. G. Pagliuso, C. Giles, R. Lora-Serrano, F. Yokaichiya, and J. L. Sarrao, *Phys. Rev. B* **69**, 144411 (2004).
- ²¹ E. Granado, B. Uchoa, R. Lora-Serrano, A. Malachias, H. Westfahl Jr., and P. G. Pagliuso, Unpublished.
- ²² Wei Bao, P. G. Pagliuso, J. L. Sarrao, J. D. Thompson, Z. Fisk, J. W. Lynn, and R. W. Erwin, *Phys. Rev. B* **62**, R14621 (2000); *ibid.* **63**, 219901 (E) (2001).
- ²³ W. Bao, P. G. Pagliuso, J. L. Sarrao, J. D. Thompson, Z. Fisk, and J. W. Lynn, *Phys. Rev. B* **64**, 020401(R) (2001).
- ²⁴ S. Chang, P. G. Pagliuso, W. Bao, J. S. Gardner, I. P. Swainson, J. L. Sarrao, and H. Nakotte, *Phys. Rev. B* **66**, 132417 (2002).
- ²⁵ R. Lora-Serrano, L. Mendonça Ferreira, D. J. Garcia, E. Miranda, C. Giles, J. G. S. Duque, E. Granado and P. G. Pagliuso, To appear in *Physica B*.
- ²⁶ C. Giles, F. Yokaichiya, S. W. Kycia, L. C. Sampaio, D. C. Ardiles-Saravia, M. K. K. Franco, and R. T. Neuenschwander, *J. Synchrotron Rad.* **10**, 430 (2003).
- ²⁷ J. P. Hill and D. F. McMorrow, *Acta Crystallogr.* **A52**, 236 (1996).
- ²⁸ P. G. Pagliuso, D. J. Garcia, E. Miranda, E. Granado, R. Lora Serrano, C. Giles, J. G. S. Duque, R. R. Urbano, C. Rettori, J. D. Thompson, M. F. Hundley, and J. L. Sarrao, To appear in *J. Appl. Phys.*
- ²⁹ R. M. Galera, M. Amara, P. Morin, and P. Burle, *J. Phys.: Condens. Matter* **10**, 3883 (1998).
- ³⁰ S. W. Lovesey and S. P. Collings, *X-Ray Scattering and Absorption by Magnetic Materials* (Oxford Science, Oxford, 1996).
- ³¹ G. Evans and R. F. Pettifer, *J. Appl. Cryst.* **34**, 82 (2001).
- ³² M. van Veenendaal, J. B. Goedkoop, and B. T. Thole, *Phys. Rev. Lett.* **78**, 1162 (1997).
- ³³ D. F. McMorrow, D. Gibbs, and J. Bohr, in *Handbook on the Physics and Chemistry of Rare Earths*, edited by K. A. G. Jr. and L. Eyring (North-Holland, Amsterdam, 1997).
- ³⁴ H. Stragier, J. O. Cross, J. J. Rehr, L. B. Sorensen, C. E. Bouldin, and J. C. Woicik, *Phys. Rev. Lett.* **69**, 3064 (1992).
- ³⁵ J. P. Hannon, G. T. Trammell, M. Blume, and D. Gibbs, *Phys. Rev. Lett.* **61**, 1245 (1988).